$\bar{p}p$ interactions at 2.32 GeV/c †

C. K. Chen, T. Fields, D. S. Rhines,* and J. Whitmore‡
Argonne National Laboratory, Argonne, Illinois 60439
(Received 21 July 1977)

A bubble-chamber experiment based on 304 000 events of $\bar{p}p$ interactions at 2.32 GeV/c is described. The film was automatically scanned and measured by the POLLY II system. Details of the data-analysis methods are given. We report results on cross sections for constrained final states, tests of C invariance, and inclusive pion and ρ^0 multiplicity parameters for annihilation final states.

I. INTRODUCTION

This paper describes a comprehensive bubble-chamber experiment on $\bar{p}p$ interactions at 2.32 GeV/c. In this study, we applied high-speed film-analysis techniques to the task of obtaining accurate and complete bubble-chamber data at a single beam momentum.

Because many reaction channels are accessible to study and since a large number of events (~304 000) were analyzed, the scope of this paper will be restricted for practical reasons to a description of the experimental data analysis procedures[1] and to a few particular physics results concerning cross sections, C-invariance tests, and multiplicities. Reports have already been given on ρ-ω interference,[2] certain two-meson final states,[3] inclusive distributions,[4] elastic scattering,[5] the $\bar{p}p\pi^+\pi^-$ final state,[6] multipion final states,[7] and the $K^+K^-\pi^+\pi^-$ final state.[8]

In the following section, the experimental details of the exposure, scanning, measuring, and event analysis are described. Then Sec. III–V give results concerning cross sections, C-invariance checks, and multiplicities.

II. EXPERIMENTAL DETAILS

Exposure

The pictures for this experiment were taken in the Argonne 30-in. hydrogen bubble chamber using antiprotons provided by the 7° electrostatically separated beam at the Zero Gradient Synchrotron. The momentum bite of the beam line was set at ±1.0%, and a total of 568 000 pictures with an average of 10 tracks per picture were taken in three separate runs.

To monitor the light-particle beam contamination (π, μ, e), a Čerenkov counter was used at the bubble-chamber entrance and set to count pions and lighter particles. When a beam pulse contained one or more Čerenkov counts, the picture was not taken. In a separate study to determine the possible effects of beam contamination by pions, 1 000 pictures of 2.32-GeV/c pions were processed through the analysis system as if it were an antiproton beam. It was found that from 10 to 50% of the pion interactions were able to kinematically fit various $\bar{p}p$ hypotheses. Since the Čerenkov veto counter reduced the effective pion beam contamination to about 0.3%, the resulting contamination in the fitted $\bar{p}p$ channels is expected to be negligible.

Magnetic field

The following method, utilizing the four-constraint annihilation events into four or six charged pions, was used to provide a direct and independent determination of the absolute value of the magnetic field: Using energy and momentum conservation and working in the lab system, we can write

$$s = 2m_p \sum_i E_i = \left(\sum_i E_i\right)^2 - \left(\sum_i \vec{p}_i\right)^2 , \tag{1}$$

where the summation is over the outgoing pions. For the correct magnetic field then

$$C = \frac{2m_p \sum_i E_i}{(\sum E_i)^2 - (\sum_i \vec{p}_i)^2} = 1 . \tag{2}$$

This quantity, which involves only the outgoing tracks, was calculated for a sample of 4π and 6π events using the measured values of the track parameters.

Figure 1 shows the result for a sample of the data. In an incorrect magnetic-field value is used, the average C observed will not be 1. With the assumption that the pions are relativistic, the relation between the magnetic field and C is given by

$$\frac{\Delta H}{H} = -\frac{\Delta \bar{C}}{\bar{C}} . \tag{3}$$

For each run, a sample of four-constraint 4π and 6π events was checked, yielding a central-magnetic-field value of 30.80 ± 0.03 kG for all three runs.

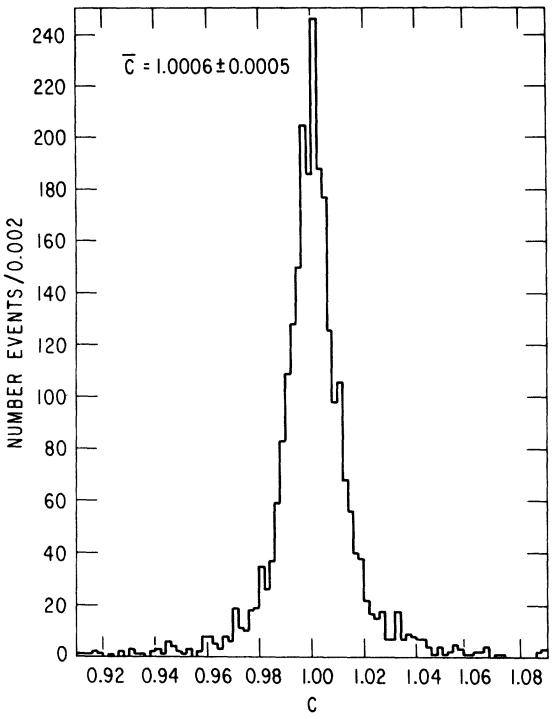

FIG. 1. Measured values of the quantity C, defined in Eq. (2), for a sample of four-constraint events.

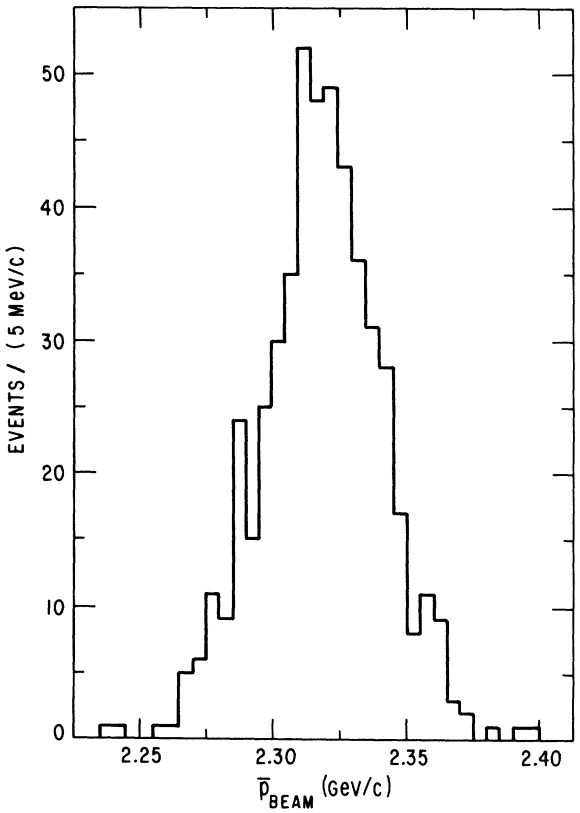

FIG. 2. Measured values of the momentum of the incident track for a sample of four-constraint events.

Beam momentum

The beam momentum has been checked for each of the three runs which constitute the entire exposure by several methods; all of the results are consistent with an average beam momentum at the center of the chamber of the chamber of 2.320 GeV/c with a dispersion (standard deviation) of ±0.025 GeV/c. The most accurate measurement was given by taking a sample of 4π or 6π events (four-constraint fits) and finding the momentum of the beam track from a kinematic fit. The beam momentum at the center of the chamber for a sample of such (non-beam-averaged) events is shown in Fig. 2.

Scanning and measuring

Most of the scanning and measuring was done automatically with POLLY II, a computer-controlled cathode-ray-tube (CRT) measuring device.[9] All 2-, 4-, 6-, 8-, and 10-prong events were measured, except that neither small-angle elastic scattering events in which the stopping proton track appeared shorter than 1 cm on the POLLY optical display (2.5 cm in projected space length) nor events with an obvious Dalitz pair were measured. Vee events have been scanned for on conventional scan tables, and measured on POLLY II in a separate pass through the film. Their analysis will be reported elsewhere. The primary vertices of the vee events were measured as nonvee events in the initial automatic scan of the film. Thus the numbers of events given here include events with a secondary vee; we have been careful to avoid any consequent double counting or contamination effects.

Since this was the first bubble-chamber experiment in which most of the events were not found by the human eye, we shall describe the data acquisition and handling in more than average detail.

Automatic scanning

To briefly describe the automatic scanning process: Track signals are found along the upstream edge of the fiducial region. These beam track candidates are followed upstream as far as possible and then back downstream through the fiducial volume. Close beam tracks separated by less than 250 μm on film and off-momentum tracks are ignored. An interaction is detected when a beam track deviates from a smooth circular path or disappears. When all beam tracks have been

TABLE I. POLLY scanning-efficiency study.

	Events found by human scanners	Events found by POLLY	POLLY biased losses
Zero-prong events	84	71	0
Elastic, $L_p < 2.5$ cm	108	86	11
Elastic, $L_p > 2.5$ cm	254	210	10
Other two-prong events	305	257	6
Four-prong events	356	296	4
Six-prong events	86	72	2
Eight-prong events	1	1	0
Total	1194	993	33
Summary of event losses			
POLLY missed (unbiased)	197		
POLLY missed (biased)	33		
Human scanners missed	29		

followed, a total path length is calculated for the accepted beam tracks within the fiducial volume. Only a single view of each picture is scanned.

Several comparisons were made between POLLY scan results and results from thorough human scanning. Table I gives results from a careful study using 1600 pictures. Unbiased losses include losses due to POLLY's failure to initially detect and follow a beam track, and close beam tracks which are not followed because they are less than 250 μm apart on the film. No correction was necessary for these losses in determining cross sections because the corresponding track length for these beam tracks was not measured. The unbiased loss was $(16.5 \pm 1.2)\%$ for this study.

A biased loss occurred when POLLY followed an acceptable beam track and failed to find its interaction. Small-angle elastic scattering presents a problem for this method of scanning. In this case, the antiproton track can appear undeflected and the event may not be detected. Other biased losses are due to undetected overlapping beam tracks or to events near the downstream end of the fiducial volume where a secondary track was mistakenly interpreted as a continuation of the beam track. For inelastic events, this study showed there was a biased scanning loss of $(1.4 \pm 0.4)\%$.

After automatic measurement of the event, the POLLY CRT displayed the measured track segments together with a request for operator assistance if measurement difficulty was encountered.

Bubble-density measurement

During track following, each POLLY slice scan consists of a group of scan lines oriented approximately at right angles to the track. POLLY recorded the number of hits (H), the number of misses (M), and the average width of each scan line crossing ($\bar{W}$), so that bubble-density information can be derived. Each view was treated independently in terms of the apparent or projected bubble density as seen on the film. The measurement of the observed bubble density was based on the lacunarity $L = M/(H+M)$. The measured bubble density was taken to be proportional to $-\ln(L)/\bar{W}$. The average crossing width was used to correct

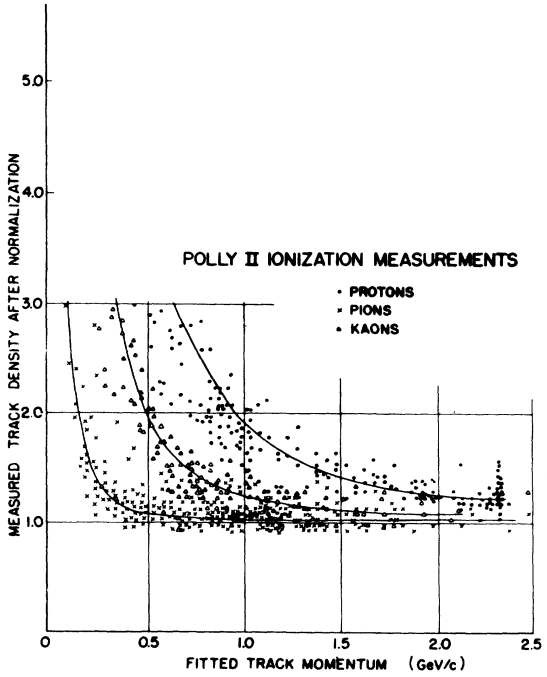

FIG. 3. Measured values of bubble density for a sample of tracks whose identity was known from kinematic fitting.

for changes in apparent bubble size along the track, such as might arise from different illumination of a track in different parts of the chamber.

For each view, a bubble density χ^2 was formed using the measured bubble density, its error, and the bubble density predicted by the kinematic fit for each track. From the sum of the χ^2 for each view, an overall bubble density χ^2 probability was derived. This probability was used in the automatic decision process, along with kinematic information, in order to select the most likely event hypothesis. Figure 3 shows typical distributions obtained from the bubble-density measurements.

Track reconstruction

The Argonne version of program TVGP first finds corresponding tracks in each view (track matching), and then geometrically reconstructs the tracks in space by doing a mass-dependent helix fit. The geometry failure rates were roughly 3% per track.

Kinematic fitting

Kinematic fitting was done in program GRIND. The correctness of error assignments in momenta and angles were checked by several methods, all of which indicated a small overestimation of the errors on the measured track parameters. These checks included the distribution of kinematic probability and stretches, the K°-mass-squared distribution and the η° width. For example, in the 5π final state, some 190 η° are observed[7] to decay to three pions with a full width at half maximum (FWHM) of 13 ± 2 MeV. This is to be compared with the resolution function calculated using the errors and correlations on the fitted track parameters which gives an expected FWHM of 16 ± 1 MeV.

The event hypotheses which were used include nonannihilation, annihilation into pions, and annihilation with kaons. Also included for each event type was the "pion no-fit" hypothesis, corresponding to annihilation to charged pions plus more than one neutral pion. About 50% of the four-prong events were assigned to the "pion no-fit" category.

Automatic hypothesis decisions

In contrast to the frequently used human-editing technique (where physicists examine kinematic-fit information and the actual pictures in order to choose the correct fit), this function was handled by program GRIND using the kinematic-fit results and the POLLY bubble-density data. The decision took place in three steps:

Step A. Only fits with reasonable kinematic χ^2 probabilities were kept ($P_{\text{kin}} > 0.02$ for $1c$ fits and $P_{\text{kin}} > 0.0001$ for $4c$ fits).

Step B. Only those fits were kept whose bubble-density χ^2 probability was at least comparable to that of the pion no-fit hypothesis [P_{bd} for fit $> 0.1\ P_{bd}$ (pions)]. If no fits were left, the pion no-fit hypothesis was kept. Fits which have a bubble density probability which is much higher than that of the pion no-fit hypothesis were flagged [$P_{bd} > 10 P_{bd}$ (pions)].

Step C. Fits were selected using the empirically chosen parameter

$$P = N^2 P_{bd} P_{\text{kin}}, \tag{4}$$

where N is the constraint of class of the fit. The best fit was kept, and up to two additional ambiguous fits were also kept if $P > 1.4P$ (best). Highly constrained fits were given heavy weight by the factor N^2.

III. CROSS SECTIONS

Cross-section basis

Event losses occurring in the data processing system have been studied carefully. Sources of loss include scanning inefficiency, POLLY operator rejects, and measurement losses. Each of these losses is given in Table II as an efficiency, defined as $(N - N_{\text{lost}})/N$, where N is the input before a given loss.

Measurement losses include, in addition to ge-

TABLE II. Cross-section basis by event type.

	2 prong	4 prong	6 prong	8 prong
Scanning efficiency $= \eta_1$	0.986	0.986	0.986	0.98
Operator rejection efficiency $= \eta_2$	0.993	0.989	0.978	0.96
Measurement efficiency $= \eta_3$	0.931	0.851	0.751	0.535
Total efficiency, $\eta_1\eta_2\eta_3$	0.911	0.830	0.724	0.503
No. of total events	175 884	106 712	20 601	406
Total cross section basis (μb/event)	0.2147	0.2238	0.2628	0.369
Systematic normalization error	$\pm 4\%$	$\pm 4\%$	$\pm 4\%$	$\pm 4\%$
Error on total efficiency	$\pm 2\%$	$\pm 2\%$	$\pm 3\%$	$\pm 4\%$

TABLE III. Topological cross sections.

Topology	Special small-angle loss	Net Dalitz-pair correlation	Cross section[a] (mb)
0 prong	1.00	1.00	6.4 ±0.05
2 prong	1.34	1.00	49.2 ±2.5
4 prong	1.00	1.00	23.8 ±1.0
6 prong	1.00	0.98	5.27 ±0.22
8 prong	1.00	0.92	0.136 ±0.010
10 prong	1.00	0.67	0.0004±0.0003
Total			84.8 ±4.0

[a]Errors include a 4% systematic normalization error.

TABLE IV. Numbers of kinematic fits (after bubble-density selections).

Constraint class	Final state	Unique[a] fit + best fit	Best fit	Less than best fit
		Two-prong events		
4	$\pi^-\pi^+$	219	•••	2
4	K^-K^+	95	3	2
4	$\bar{p}p$	69 651	627	278
1	$\pi^+\pi^-\pi^0$	3 427	578	536
1	$\pi^+\pi^-\eta^0$	2 376	972	2152
1	$\pi^+\bar{p}n$	10 924	435	601
1	$p\pi^-\bar{n}$	9 884	88	86
1	$p\bar{p}\pi^0$	10 359	439	294
1	$K^+\pi^-K^0$	6 758	1440	1728
1	$\pi^+K^-K^0$	2 687	1125	1824
1	$K^+K^-\pi^0$	3 263	972	1381
0	$\pi^+\pi^-$(MM)	56 241	•••	•••
		Four-prong events		
4	$2\pi^-2\pi^+$	6 247	14	8
4	$K^-K^+\pi^-\pi^+$	1 296	77	75
4	$\bar{p}p\pi^+\pi^-$	4 906	16	9
1	$2\pi^-2\pi^+\pi^0$	28 036	546	701
1	$2\pi^-2\pi^+\eta^0$	11 001	1766	1767
1	$K^\pm\pi^\mp\pi^+\pi^-(K^0)$	13 141	3129	3688
1	$K^+K^-\pi^+\pi^-\pi^0$	6 370	1684	2324
1	$\bar{p}p\pi^+\pi^-\pi^0$	39	1	•••
0	$2\pi^-2\pi^+$(MM)	35 676	•••	•••
		Six-prong events		
4	$3\pi^+3\pi^-$	3 932	8	1
4	$K^+K^-2\pi^+2\pi^-$	208	14	21
1	$3\pi^+3\pi^-\pi^0$	9 071	5	10
1	$K^+K^-2\pi^+2\pi^-\pi^0$	257	76	83
1	$K^\pm\pi^\mp2\pi^+2\pi^-(K^0)$	573	72	104
0	$3\pi^+3\pi^-$(MM)	6 560	•••	•••
		Eight-prong events		
4	$4\pi^+4\pi^-$	152	•••	•••
1	$4\pi^+4\pi^-\pi^0$	128	•••	•••
0	$4\pi^+4\pi^-$(MM)	126	•••	•••

[a]A unique fit means that unique track-mass assignments as well as a particular final state were selected.

ometry failures, events which have one or more track parameters unmeasured, as happens, for example, when an outgoing track scatters close to the vertex. Normal one-constraint fits could then no longer be obtained. To obtain a cross-section basis which applies equally to both one-constraint and normal four-constraint fits, the requirement was made that all track parameters be measured. When this requirement was not met, for the purposes of cross-section determination an event was then treated as lost.

Topological and total cross sections

The topological-cross-section results were determined from a particular portion of the film from the second half of the run. Automatic scanning and other aspects of the data handling were operating in an optimum way for this portion.

The determination of the number of unmeasured small-angle elastic scattering events is based on a careful extrapolation of the measured elastic angular distribution to $t=0$ and has been described elsewhere.[5] The net result is to add an amount (11.6 ± 1.5) mb to the observed two-prong cross section. This corresponds to ~60 000 elastic events whose recoil-proton tracks were too short to satisfy the scanning acceptance criteria.

To determine the zero-prong cross section, several special automatic scans were conducted on POLLY II using a total of ten rolls of film.

Small corrections were necessary for the failure of POLLY operators to identify Dalitz pairs (~80% of these pairs were identified correctly). These corrections were estimated by searching for low-mass (<20 MeV) enhancements for positive and negative pairs of tracks treated as electrons. These events were found not to contaminate fitted channels in any significant way.

The resulting topological and total cross sections are summarized in Table III. Our total-cross-section result is in good agreement with (84.8 ± 0.9) mb measured in a counter experiment by Abrams *et al.*[10]

Cross sections for individual final states

Table IV lists the numbers of events which fitted various hypotheses, for two-, four-, six-, and eight-prong events. It can be seen that the four-constraint (4C) fits are rather free of serious ambiguity problems, as would be expected. The validity of the 4C fits was studied by careful kinematic analysis of the $\pi^-\pi^+$ and K^-K^+ final states, where the 4C signals represent only about 0.1% of the background events. The result was that even in these final states, the 4C fits form a valid and rather pure sample.

Two principal kinds of contamination which must be considered for the 1C events are ambiguities with other 1C and with no-fit hypotheses, and the misclassification of common 4C event types, particularly elastic scattering. Table IV shows that the size of the kinematic ambiguity problem ranges

TABLE V. Cross sections.

Final state	Number of events	All track parameters measured	Loss of 4C fits	Contamination from 4C	Net effect 1C ambig. and no-fit contam.	Special short-track small-angle losses	Cross section (mb)	Estimated[a] error in cross section (mb)
$\pi^-\pi^+$	219	1.00	1.02	1.00	1.00	1.02	0.049	0.004
K^-K^+	95	0.98	1.04	1.00	1.00	1.04	0.021	0.002
$\bar{p}p$	69 651	0.99	1.13	1.00	1.00	1.77	29.0	1.5
$\pi^+\pi^-\pi^0$	3 427	1.00	1.00	0.926	0.949	1.00	0.65	0.04
$\pi^+\bar{p}n$	10 924	1.00	1.00	0.841	0.853	0.98	1.65	0.11
$\pi^-p\bar{n}$	9 884	1.00	1.00	1.00	0.777	1.00	1.65	0.11
$\bar{p}p\pi^0$	10 359	1.00	1.00	1.00	0.958	0.99	2.11	0.13
$2\pi^-2\pi^+$	6 247	0.984	1.084	1.00	1.00	1.00	1.49	0.09
$K^-K^+\pi^-\pi^+$	1 296	0.936	1.05	1.00	1.00	1.05	0.30	0.02
$\bar{p}p\pi^+\pi^-$	4 906	0.983	1.03	1.00	1.00	1.00	1.11	0.07
$2\pi^-2\pi^+\pi^0$	28 036	1.00	1.00	1.00	0.959	1.00	6.02	0.4
$\bar{p}p\pi^+\pi^-\pi^0$	39	1.00	1.00	1.00	1.00	1.00	0.0088	0.0016
$3\pi^-3\pi^+$	3 932	0.973	1.133	1.00	1.00	1.00	1.14	0.08
$K^-K^+2\pi^-2\pi^+$	208	0.860	1.140	1.00	1.00	1.08	0.058	0.006
$3\pi^-3\pi^+\pi^0$	9 071	1.00	1.00	1.00	1.026	1.00	2.45	0.16
$4\pi^-4\pi^+$	152	0.960	1.185	1.00	1.00	1.00	0.064	0.007
$4\pi^-4\pi^+\pi^0$	128	1.00	1.00	1.00	1.156	1.00	0.055	0.006

[a] Including the 4% normalization error.

from small for $\bar{N}N\pi$, 5π, and 7π fits to large for 1C fits with kaons.

The data described above have been used to obtain cross sections for the 17 final states listed in Table V. Several correction factors are shown in Table V which were required to take account of the following effects:

(a) Adjustment of 4C channels for fits obtained with one or more track parameters unmeasured, as discussed above.

(b) Loss of 4C fits due to systematic errors associated with short tracks and other special situations. This problem has been studied carefully[5] for the elastic events, resulting in the reclassification to elastic of ~9 400 events from the 106 000 two-prong events which did not give an elastic 4C fit, making a total of ~79 000 measured elastic scattering events.

(c) Contamination in 1C categories from events which did not fit in their proper 4C category (almost entirely elastic events).

(d) Effect of ambiguities with 1C hypotheses, unfittable final states, and vee events. This correction was evaluated from the background under the missing mass peaks.

(e) Special small-angle and short-track losses (including the small-angle scanning loss for elastic scattering described above), and losses from charged-kaon decay.

Final states corresponding to highly ambiguous 1C fits are not listed in Table V, since the required corrections are large and in most cases uncertain.

IV. C INVARIANCE

If charge-conjugation invariance is satisfied in $\bar{p}p$ reactions, the π^- and π^+ c.m. angular distributions should be forward-backward reflections of each other and the π^0 or other neutral system c.m. angular distribution should be forward-backward symmetric.[11]

We have examined several constrained final states including $2\pi^+2\pi^-$, $2\pi^+2\pi^-\pi^0$, $3\pi^+3\pi^-$, $3\pi^+3\pi^-\pi^0$, and $\bar{p}p\pi^+\pi^-$ for compatibility with these expectations. Typical results are shown in Figs. 4–6. There is generally good agreement with the expected symmetry, except for a small deviation near 0° in Fig. 5.

This small deviation can probably be attributed to a systematic loss of 1C fits due to secondary interactions of slow backward π^+ tracks. The π^+p cross section is large for these tracks (~200 mb), much larger than that for forward π^-. Events with a track scattering close to the vertex are measured as two-point tracks, and since this gives no momentum measurement, 1C fits could not be ob-

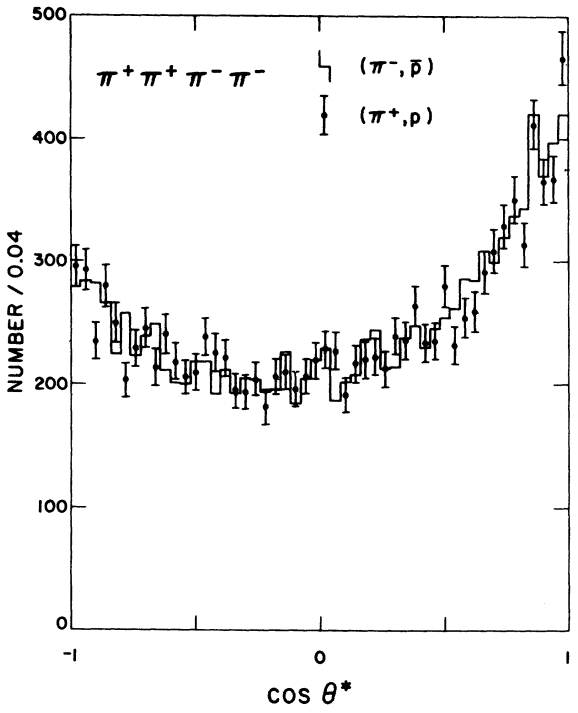

FIG. 4. Center-of-mass angluar distributions of pions in the $\pi^+\pi^+\pi^-\pi^-$ final state.

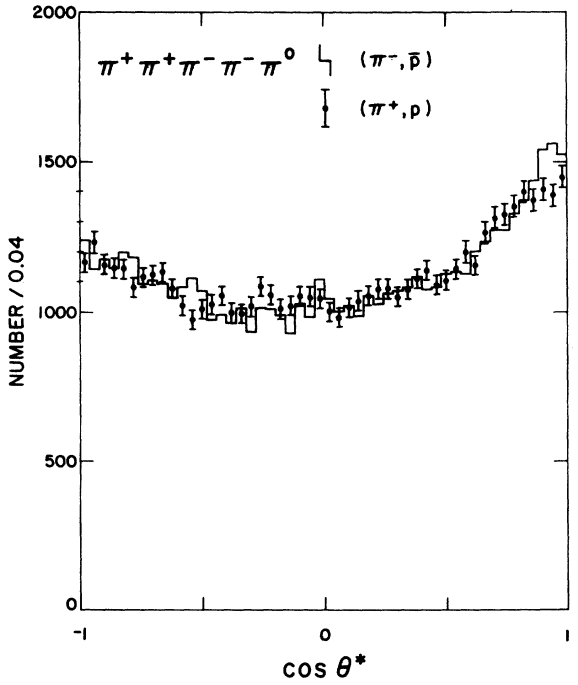

FIG. 5. Center-of-mass angular distributions of charged pions in the $\pi^+\pi^+\pi^-\pi^-\pi^0$ final state.

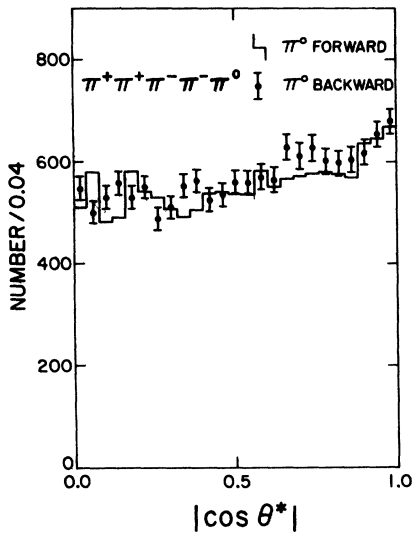

FIG. 6. Neutral-pion c.m. angular distribution in the $\pi^+\pi^+\pi^-\pi^-\pi^0$ final state.

tained.

As described by Baltay *et al.*,[12] the experimental data can be used to set a limit on the relative amplitude α of a possible C-nonconserving part of the annihilation interaction from the equation

$$\alpha \leq \left(\frac{(2N_B)^{1/2}}{N_{\text{counts}}}\right)^{1/2}, \tag{5}$$

where N_B is the number of bins. For the total data which we have used, $N_{\text{counts}} \approx 10^5$ and $N_B \approx 200$, so that our result is $\alpha \leq 0.014$ for annihilation into exclusive pion channels. This is similar to the result of Baltay *et al.*

We have described elsewhere[8] a number of detailed C-invariance tests using data from kaon final states.

V. ANNIHILATION MULTIPLICITIES

In the following subsections, we report pion multiplicities, correlation coefficients, and ρ^0/ω^0 multiplicities as observed in the annihilation part of the $\bar{p}p$ cross section. Such data are important for testing models of the annihilation process,[13,14] and can also be compared with results from e^+e^- annihilation and high-energy pionization processes.

Charged-pion multiplicities

Two principal effects must be accounted for in order to obtain pion annihilation multiplicity data from the topological cross sections given in Table III. First, the contributions of nonannihilation channels must be subtracted. This can be done in a fairly straightforward way, using published cross sections[15] as well as individual channel cross sections from Table V. However, the zero-prong and two-prong events are dominated by nonannihilation reactions, so that the resulting uncertainties in the corresponding annihilation cross sections are significant. The third column of Table VI shows the estimated nonannihilation cross sections.

The second principal effect involves events with kaons in the final state. As mentioned above, the overall topological cross sections of Table III include events with associated vees. We shall define the mean pion multiplicity to exclude contributions from events with kaons in the final state. The estimated cross sections for kaon events are shown in the fourth and fifth column of Table VI. These estimates were based on the number of observed events with vees and to a lesser degree of the number of kinematic fits to charged-kaon hypotheses.

From Table VI, we also obtain the cross-section results: σ (annihilation) = 42.7 ± 2.5 mb, σ (pion annihilation) = 35.4 ± 3.0 mb, and σ (kaon annihilation) = 7.2 ± 1.2 mb.

Using the cross sections given in Table VI for annihilations into pions, we obtain $\langle n_- \rangle = 1.88 \pm 0.09$ and $f_2^{--} = \langle n_-(n_- - 1)\rangle - \langle n_-\rangle^2 = -1.43 \pm 0.13$. These results are consistent with the trend of those of other annihilation experiments. The nega-

TABLE VI. Cross sections for obtaining charged multiplicity.

Number of prongs	Total (mb)	Estimated nonannihilation (mb)	Annihilation with visible vee (mb)	Kaon annihilation without visible vee (mb)	Remainder: annihilation into pions (mb)
0	6.4 ±0.5	6 ±1	0.10 ±0.02	0.07 ±0.02	0.2 ±1.2
2	49.2 ±2.5	35 ±2	1.5 ±0.2	3.5 ±1.0	9.2 ±2.5
4	23.8 ±1.0	1.12±0.07	0.5 ±0.1	1.5 ±0.5	20.7 ±1.0
6	5.27 ±0.22	0	0.015±0.005	0.050±0.015	5.21 ±0.22
8	0.136 ±0.010	0	0	0	0.136 ±0.010
10	0.0004±0.0003	0	0	0	0.0004±0.0003
Total	84.8 ±4.0	42.1 ±2.2	2.1 ±0.22	5.1 ±1.1	35.4 ±3.0

TABLE VII. Associated π^0 multiplicities in pion annihilation.

Prong number	Pion annihilation cross section (mb)	$\langle n_{\pi^0} \rangle$
0	0.2 ±1.2	4 ±1
2	9.2 ±1.5	3.0±0.5
4	20.7 ±1.0	1.9±0.2
6	5.2 ±0.2	1.1±0.2
8	0.14 ±0.01	0.5±0.2
10	0.0004±0.0003	0

tive value of f_2^{--} means that the multiplicity distribution in n_- is narrower than a Poisson distribution; its quantitative interpretation has been discussed elsewhere. In general terms, the meaning of f_2^{--} can be understood by noting[13] that if the overall multiplicity distribution is Poisson, and if the distribution in charged and neutral pions is binominal, then $f_2^{--} = -\frac{1}{2}\langle n_- \rangle$. Energy-momentum conservation will further narrow the n_- distribution, yielding $f_2^{--} \cong -0.61\langle n_- \rangle$.

Neutral-pion multiplicities

The average number of π^0 for an n-prong multi-π^0 event can be estimated by dividing the average missing energy per event by the estimated average π^0 energy. Study of the $2\pi^+2\pi^-\pi^0$ and $3\pi^+3\pi^-\pi^0$ events showed[7] that the mean π^0 energies were, respectively, 0.978 and 0.924 of the mean charged-pion energies, and we assumed that similar fractions also apply to the multineutral events.

For the $2\pi^+2\pi^-$ MM events, this procedure yielded $\langle \pi^0 \rangle = 2.6 \pm 0.1$. This result agrees with that obtained at 2.5 GeV/c (Ref. 16) using an alternate procedure of fitting the missing-mass spectrum to a sum of Lorentz-invariant phase-space spectra with 2, 3, 4, and $5\pi^0$'s.

However, several major difficulties are encountered in using this method to obtain precise values for $\langle n_{\pi^0} \rangle$ as a function of n_-. These include the absence of a charged-pion spectrum for zero-prong events, the large number of zero-prong and two-prong nonannihilation events, the significant fraction of kaon final states for two-prong events in particular, and poor knowledge of η^0 production. We have made estimates of these effects using pertinent data from this experiment and others, yielding the results shown in Table VII. From these results, we obtain $\langle n_{\pi^0} \rangle = 2.1 \pm 0.2$ and $f^{-0} = \langle n_- n_0 \rangle - \langle n_- \rangle \langle n_0 \rangle = -0.45 \pm 0.12$.

Interpretation of neutral-pion multiplicity results in terms of statistical models of annihilation has been extensively discussed elsewhere.[17] Most experiments indicate that $\langle n_{\pi^0} \rangle$ exceeds $\langle n_{\pi^-} \rangle$. For example, the heavy-liquid bubble-chamber experiment at 1.6 GeV/c of Fett *et al.*,[18] in which the γ rays from π^0 decay were detected with good efficiency, has yielded preliminary results also indicating that $\langle n_{\pi^0} \rangle$ exceeds $\langle n_{\pi^-} \rangle$ by $(16 \pm 5)\%$. Further progress in accurately measuring neutral-pion multiplicities will probably require the use of track-sensitive-target bubble-chamber techniques.

ρ^0 and ω^0 multiplicities

Many of the pions produced in annihilation are decay products of higher-mass mesons. For events with no more than one missing π^0, useful information on the production of such higher-mass mesons can be obtained from the analysis of invariant-mass spectra, using maximum-likelihood computer programs to estimate the associated production of resonances and the reflections of

TABLE VIII. ρ^0 and ω^0 production rates.

Final state	Cross section (mb)	ρ^0/event	$\sigma_{\rho 0}$ (inclusive) (mb)	ω^0/event	$\sigma_{\omega 0}$ (mb)[a]
Neutral	0.2 ±1.2	0	0		
$\pi^+\pi^-$	0.049±0.004	0	0		
$\pi^+\pi^-\pi^0$	0.65 ±0.04	0.08±0.02	0.051±0.015		
$\pi^+\pi^-$MM	8.5 ±2.5	0.15±0.07	1.3 ±0.6		
$2\pi^+2\pi^-$	1.49 ±0.09	0.60±0.05	0.89 ±0.08		
$2\pi^+2\pi^-\pi^0$	6.02 ±0.40	0.43±0.04	2.6 ±0.3	0.20±0.02	1.34±0.15
$2\pi^+2\pi^-$MM	13.2 ±1.2	0.20±0.02	2.6 ±0.4		
$3\pi^+3\pi^-$	1.14 ±0.08	1.1 ±0.2	1.3 ±0.3		
$3\pi^+3\pi^-\pi^0$	2.45 ±0.16	0.6 ±0.1	1.5 ±0.3	0.65±0.05	1.77±0.17
$3\pi^+3\pi^-$MM	1.6 ±0.2	0.5 ±0.3	0.8 ±0.5		
$4\pi^+4\pi^-$	0.064±0.007	0.8 ±0.3	0.05 ±0.02		
$4\pi^+4\pi^-\pi^0$	0.055±0.006	0.8 ±0.3	0.04 ±0.02	1.0 ±0.3	0.06±0.02

[a]Corrected to include all decay modes of ω^0.

resonance production on other mass spectra. However, because of the simplifying assumptions required in such analyses, the large combinatorial backgrounds for events of high charged multiplicity, and the fact that (at 2.3 GeV/c) some (66±7)% of the pion annihilations have two or more missing π^0's, it is not possible to obtain inclusive data on meson resonance production in this way.

However, the study of inclusive ρ^0 production is experimentally straightforward, because of the ~100% branching ratio for $\rho^0 \to \pi^+\pi^-$. We have listed in Table VIII the observed ρ^0 signal in the $\pi^+\pi^-$ spectra for pion-annihilation final states. Most of these results are described in Ref. 7.

From these results, the inclusive cross section for annihilation into ρ^0 + pions is 11 ± 2 mb. If we assume that $\langle\rho^+\rangle = \langle\rho^-\rangle = \langle\rho^0\rangle$, we conclude that (33 ± 7)% of the charged pions from pion annihilation are decay products of ρ mesons.

Comparison of ω^0 production with ρ^0 production is a matter of substantial interest but can only be done for a few specific final states, as listed in Table VIII. We see that the ratio $\sigma(\omega^0 X)/\sigma(\rho^0 X)$ is measured to be 1.5 ± 0.2 for $X = \pi^+\pi^-$, 1.5 ± 0.4 for $X = 2\pi^+2\pi^-$, and 1.2 ± 0.6 for $X = 3\pi^-3\pi^+$. If the ω^0 inclusive production cross section is 1.5 times that for ρ^0, then 25% of the charged pions from pion annihilation are ω^0 decay products.

ACKNOWLEDGMENTS

We wish to record our thanks to the many persons who participated in the various phases of this experiment. The POLLY system was developed to the required operational state by Don Hodges, Richard Royston, Bruce Phillips, Bob Zieman, Frank Beck, Wade Allison, and Jim Loken. The physics analysis depended on important contributions from Yona Oren, Steven Egli, Allen Cooper, and Wade Allison.

---

†Work supported by the U. S. Energy Research and Development Administration.

*Present address: E-Systems, Inc., Garland, Texas 75222.

‡Present address: Michigan State University, East Lansing, Michigan 48824.

[1]A more complete description of the data analysis procedures can be found in D. Rhines, Argonne Report No. ANL/HEP 7146, 1971 (unpublished).

[2]T. Fields *et al.*, Phys. Rev. Lett. 27, 1749 (1971).

[3]T. Fields *et al.*, Phys. Lett. 40B, 503 (1972).

[4]T. F. Hoang *et al.*, Nucl. Phys. B38, 62 (1972); Phys. Rev. Lett. 27, 1681 (1971).

[5]W. W. M. Allison *et al.*, Nucl. Phys. B56, 1 (1973).

[6]Y. Oren *et al.*, Nucl. Phys. B53, 269 (1973).

[7]Y. Oren *et al.*, Nucl. Phys. B71, 189 (1974).

[8]C. K. Chen *et al.*, Nucl. Phys. (to be published).

[9]W. W. M. Allison *et al.*, Nucl. Instrum. Methods 84, 129 (1970).

[10]R. J. Abrams *et al.*, Phys. Rev. D 1, 1917 (1970).

[11]A. Pais, Phys. Rev. Lett. 3, 242 (1959).

[12]C. Baltay *et al.*, Phys. Rev. Lett. 15, 591 (1965).

[13]H. I. Miettinen, in *Proceedings of the Symposium on Antinucleon-Nucleon Interactions, Prague, 1974*, edited by L. Montanet (CERN, Geneva, 1974).

[14]T. Fields, in *Proceedings of the Symposium on Antinucleon-Nucleon Interactions, Prague, 1974* (see Ref. 13), p. 151.

[15]J. Enstrom *et al.*, LBL Report No. LBL-58, 1972 (unpublished).

[16]J. Clayton *et al.*, Nucl. Phys. B30, 605 (1971).

[17]C. J. Hamer, Nuovo Cimento 12A, 162 (1972); S. J. Orfanidis and V. Rittenburg, Nucl. Phys. B59, 570 (1973).

[18]E. Fett *et al.*, Phys. Lett. 59B, 182 (1975).